Ecological Modelling 222 (2011) 2663–2675

Contents lists available at ScienceDirect

Ecological Modelling

journal homepage: www.elsevier.com/locate/ecolmodel

Adding complex trophic interactions to a size-spectral plankton model: Emergent diversity patterns and limits on predictability

Neil S. Banas*

Applied Physics Laboratory, Box 355640, University of Washington, Seattle, WA 98195, USA

ARTICLE INFO

Article history:
Received 11 December 2010
Received in revised form 7 May 2011
Accepted 11 May 2011
Available online 14 June 2011

Keywords:
Phytoplankton
Zooplankton
Size spectra
Diversity
Coexistence
Predictability

ABSTRACT

A new model in the NPZ (nutrient–phytoplankton–zooplankton) style is presented, mechanistically simple but with 40 size classes each of phytoplankton (1–20 μm) and small zooplankton (2.1–460 μm), in order to resolve one level of trophic interactions in detail. General, empirical allometric relationships are used to parameterize both the optimal prey size and size selectivity for each grazer class, as is rarely done. This inclusion of complex predator–prey linkages and realistic prey preferences yields a system with an emergent pattern of phytoplankton diversity consistent with global ocean observations, i.e., a parabolic relationship between diversity (as measured by the Shannon evenness) and biomass. It also yields significant long-term time evolution, which places limits on the extent to which the community response to nutrient forcing can be predicted from forcing in a pragmatic sense. When a simple annual cycle in nutrient supply is repeated exactly for many years, transient fluctuations up to a factor of two in spring bloom magnitude persist for 10–20 years before a stable seasonal biomass cycle is achieved. When the amplitude of the nutrient-supply annual cycle is given a random interannual modulation, these long-lived transients add significant noise to a 100-year correlation between annual-mean nutrient supply and annual-mean biomass. This noise is 20% of total interannual variance in the model base case, and ranges from 0% to 40% depending on the grazer size selectivity. In general, unpredictability on the bloom timescale is damped when food-web complexity is increased by making grazers less selective, while unpredictability on the interannual scale shows the opposite pattern, increasing with increasing food-web complexity up to a high threshhold, past which community structure and biomass time evolution both suddenly simplify. These results suggests a new strategy for ensemble ecosystem forecasting and uncertainty estimation, analogous to methods common in circulation and climate modeling, in which internal variability (predator–prey interactions in the biological case; eddies and climate-system oscillations in the physical case) are resolved and quantified, rather than suppressed.

1. Introduction

Natural plankton communities are far more diverse than even a very complicated numerical model can account for (Hutchinson, 1961; Sournia et al., 1991). This diversity is crucial to the role of the plankton in marine food webs and biogeochemical cycles, and for at least two decades the ocean modeling community has been using a variety of approaches to better capture it, as reviewed further below. This study uses an idealized, size-spectral, nutrient–phytoplankton–zooplankton (NPZ) model to explore an aspect of planktonic diversity that has generally been underrepresented in this work: structure and variation in zooplankton prey preferences, i.e., the landscape of what eats what among the plankton.

Studies relating food-web complexity to community structure and function have a long history in theoretical biology (e.g., McCann et al., 1998; Chen and Cohen, 2001; Kondoh, 2003), but most contemporary plankton models derive from other lineages (Gentleman et al., 2003). Diversity-resolving planktonic ecosystem models can be sorted into two families, and recent results in both of these provide the motivating questions for this study. The first, size-spectral models (Moloney and Field, 1991; Gin et al., 1998; Baird and Suthers, 2007; Stock et al., 2008; Fuchs and Franks, 2010), map planktonic diversity onto a single variable, body size, and use allometric power laws to set growth rates, nutrient/light/prey response parameters, and so forth for each size class. Baird and Suthers (2007) demonstrated the need to resolve the size spectrum with a sufficient number of size classes to avoid mathematical artifacts, and demonstrated the rich, semi-chaotic behavior that becomes possible when phytoplankton, microzooplankton, and mesozooplankton are all included with detail and care. Poulin and Franks (2010) presented an idealized model that demonstrated the

* Corresponding author. Tel.: +1 206 685 5184.
E-mail address: neil@apl.washington.edu

0304-3800/$ – see front matter © 2011 Elsevier B.V. All rights reserved.
doi:10.1016/j.ecolmodel.2011.05.018

importance of top-down control in shaping biomass size spectra in the ocean, and also found constraints on the particular allometric power laws that yield biomass spectra consistent with reality, a step toward linking the "free" or empirical parameters that define a size-spectral model to the ecosystem structure and function the model predicts. Still, these and other size-spectral models have continued to treat predator–prey interactions relatively simply, e.g., by allowing only one prey class per predator, or using a single predator–prey size ratio, instead of letting this optimal size ratio itself vary allometrically.

Sometimes the simplification of trophic interactions in such models is very much by design: Armstrong (2003) proposed a hybrid method that specially constructs the zooplankton size spectrum to ensure a temporally smooth solution. Poulin and Franks (2010) similarly focused on steady-state solutions of their model, and assumed a continuous biomass size spectrum with a definable slope. Such approaches are appropriate to large-scale biogeochemical applications, where transient predator–prey oscillations might well be considered noise, but for other applications like harmful algal blooms or coastal food-web dynamics, where time evolution and the interplay of bottom-up and top-down controls may be of great interest, it is limiting. The model design in this study is based on the idea that grazer prey preferences can be treated with detail and empiricism equal to that used for vital rates and other physiological parameters; and that whatever chaotic or disequilibrium phenomena result should be accepted as potentially important parts of the solution.

The second broad class of diversity-resolving models avoids a reliance on allometry (which is an incomplete representation of diversity at best), and instead uses natural-selection or optimization principles to let parameter values emerge dynamically from the model solution, rather than being imposed a priori. For example, Follows et al. (2007) seeded a global ocean model with many *Prochlorococcus*-like phytoplankton classes, with temperature- and light-response parameters chosen randomly from an empirically chosen range. Competition among these random variants yielded an emergent biogeography reflecting bottom-up controls on the phytoplankton. Goebel et al. (2010) adapted this approach to model small and large phytoplankton in the California Current System. Bruggeman and Kooijman (2007) present a model written in terms of a continuous, trait-based representation of a phytoplankton community whose dynamics are based even more explicitly on biological optimization principles. What remains unclear is whether these optimization/natural-selection approaches can be extended in the same terms to the representation of zooplankton grazing and higher trophic levels (Mariani and Visser, 2010) suggests one direction. The new model experiments discussed in this paper suggest that in fact inclusion of well-resolved diversity among grazers may have a fundamentally different effect from inclusion of phytoplankton physiological diversity, working against rather than supporting the emergence of a stable, optimal plankton community, and placing fundamental limits on predictability of ecosystem dynamics (Baird, 2010).

The next section describes the model design and parameterization. Section 3.1 discusses the model's behavior under steady nutrient forcing. Since this model is run, for clarity, in an extremely simple testbed, instead of comparing it with observations from any particular location, I use integral metrics of ecosystem function to establish that this model has sufficient realism (i.e., lack of pathology) to proceed, and then discuss emergent patterns of community structure. Section 3.2 then uses test cases involving seasonal and interannual variation in nutrient supply to demonstrate the emergence of limits on ecosystem predictability, and to demonstrate the central role of the grazer prey preferences in defining the level of unpredictability.

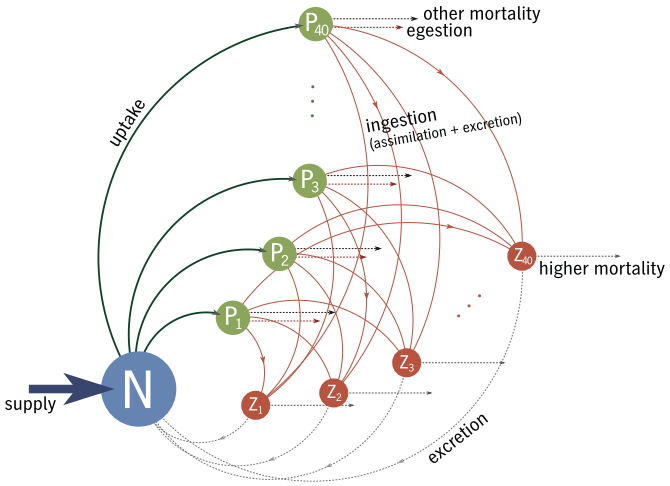

Fig. 1. Schematic of the ASTroCAT model. Circles represent nitrogen stocks, arrows indicate nitrogen fluxes.

2. The model

2.1. Model formulation

The model, named ASTroCAT (Allometric/Stochastic Trophic Complexity Analysis Tool), is schematized in Fig. 1. It uses nitrogen as its currency (stocks are reported in units of μmol N m^{-3}, or μM), with compartments for dissolved nutrients (N), 40 size classes of phytoplankton (P), and 40 classes of small zooplankton (Z). The version used here has been kept mechanistically minimal, containing only a single bottom-up control (nutrient limitation of P growth), a single top-down control (higher predation on Z), and one highly resolved level of trophic interactions (P–Z) in between. There is no light or temperature dependence to P growth, and no distinction made between the rate and timing of phytoplankton cell growth and the rate and timing of uptake of the limiting nutrient.

The physical testbed is a single box, and the detrital pool and regeneration pathways are not tracked: mortality and zooplankton egestion (sloppy feeding) are treated as losses from the model nitrogen pool, and whatever fraction of these losses is ultimately regenerated is folded into an imposed, external nutrient supply (S). Thus the model can be thought of as an "open" or "flowthrough" NPZ system, as opposed to the classical "closed" NPZ system (Franks, 2002), which sends mortality and egestion losses directly back into the N pool.[1] The minimalism of this model configuration makes the interpretation of results easier, but for a realistic application, one would, at a minimum, add light-dependence to phytoplankton growth, resolve at least one spatial dimension in the domain, and explicitly track detritus.

The model equations are as follows:

$$\frac{dP_i}{dt} = \mu_0^i \frac{N}{k_s^i + N} P_i - \sum_j \mathrm{graz}_{ij} - m\mu_0^i P_i \quad (1)$$

$$\frac{dZ_j}{dt} = \varepsilon \sum_i \mathrm{graz}_{ij} - \zeta Z_j Z_{\mathrm{tot}} \quad (2)$$

[1] The closed formulation implicitly assumes that regeneration is local and instantaneous, and uses the initial *stock* of total nitrogen as an imposed forcing parameter. The open formulation assumes that regeneration is complicated and happens elsewhere (e.g., Plattner et al. (2005)), and uses the *flux* of new and regenerated nitrogen from below or outside as the forcing parameter. This open formulation is motivated by highly advective systems like upwelling zones.

$$\frac{dN}{dt} = S - \sum_i \mu_0^i \frac{N}{k_s^i + N} P_i + (1 - \varepsilon - f_{eg}) \sum_j \sum_i graz_{ij} \quad (3)$$

P_i and Z_j are the ith and jth phytoplankton and zooplankton classes. (For clarity, a subscript i always denotes a phytoplankton size class and j a zooplankton class. See Table 1 for a summary of all symbols used.) Phytoplankton population growth (1) is a balance between (i) nutrient uptake (i.e., growth), controlled by a maximum growth rate μ_0^i and a nutrient half-saturation k_s^i; (ii) grazing; and (iii) non-grazing mortality, written as a fraction $m \approx 0.1$ of the maximum uptake rate (cf. Ref. Moloney and Field, 1991). Zooplankton population growth (2) is a balance between assimilation of ingested phytoplankton (a growth efficiency ε times total grazing) and mortality, i.e., higher predation. This mortality closure term is quadratic (Edwards and Yool, 2000), implicitly assuming that the stock of predators on Z_j is proportional to the total zooplankton stock $Z_{tot} \equiv \sum_j Z_j$. Finally, the N budget (3) is a balance between the imposed nutrient supply S, uptake by P, and a fraction of total grazing representing excretion by Z. If one imagines S to represent an advective input from or diffusive exchange with a subsurface nutrient pool, then for physical consistency one must consider the corresponding loss of P and Z to dilution. These losses are small compared with the P and Z mortality terms, however, as estimated using observations from the Oregon-Washington upwelling zone (Hickey et al., 2010), and so in order to avoid the introduction of another free parameter, these dilution losses have been omitted.

Two parameters, ε and the egestion fraction f_{eg}, control the partitioning of total grazing $graz_{ij}$ into assimilation (to Z_j), excretion (to N), and egestion (to the unmodeled detrital pool, i.e., a loss from the system). For simplicity, I have set $\varepsilon = f_{eg} = 1/3$, representing an equal partitioning among the three. Hansen et al. (1997) report that $\varepsilon \approx 0.3$ for a wide range of zooplankton, and that it does not appear to vary allometrically.

Grazing of the ith phytoplankton class by the jth zooplankton class is given by

$$graz_{ij} = I_0^j \frac{\varphi_{ij} P_i}{K_s^j + \sum_i \varphi_{ij} P_i} Z_j \quad (4)$$

where I_0^j is the maximum ingestion rate, K_s^j is the prey half-saturation level, and φ_{ij} is the relative preference of Z_j for prey type P_i. Prey preference is assumed to vary with prey size x_{prey}^i in a log-Gaussian distribution around the optimal prey size for each grazer $x_{prey\ opt}^j$:

$$\varphi_{ij} = \exp\left[-\left(\frac{\log_{10} x_{prey}^i - \log_{10} x_{prey\ opt}^j}{\Delta x_{prey}} \right)^2 \right] \quad (5)$$

The width of the Gaussian is controlled by a prey size tolerance parameter Δx_{prey} (which has units of $\log x$, not x). Eq. (5) gives the base-case, allometric formulation of the prey preferences; results are also discussed in Section 3.1.3 for a variant, stochastic formulation given by

$$\varphi_{ij}^{stoch} = \varphi_{ij} \exp(r\mathbf{R}) \quad (6)$$

where $\mathbf{R}$ is a normally distributed random variable with variance 1, and r is a free "stochasticity" parameter.

2.2. Allometric parameterization

The allometric dependence of μ_0^i, I_0^j, k_s^i and $x_{prey\ opt}^j$ on body size is given in Table 2, along with the review studies used to determine these power laws. Body sizes are specified as equivalent spherical diameter (ESD). Note that these allometric laws are simply imposed in ASTroCAT as empirical facts, in contrast to studies that attempt to model the biological processes that give rise to this allometry in the first place (Weitz and Levin, 2006; Troost et al., 2008). The vital rates μ_0^i and I_0^i show strong and similar falloff with increasing body size, according to the reviews by Tang (1995) and Hansen et al. (1997). Note that within any given size class, around these log-linear regressions, μ_0^i and I_0^i vary by approximately an order of magnitude (Fig. 2a). Eppley et al. (1969) report even greater variance around the allometric trend for nutrient half-saturation k_s^i – at the 95% confidence level, the scale coefficient is uncertain by a factor of 30 (0.01–0.3 μM N, with a power-law exponent 0.6–1.3) – and so for simplicity I have approximated this scaling as $k_s^i = 0.1 x_i$. Hansen et al. (1997) found that prey half-saturation K_s has essentially no allometric dependence, although within every functional group surveyed it varies by almost two orders of magnitude.

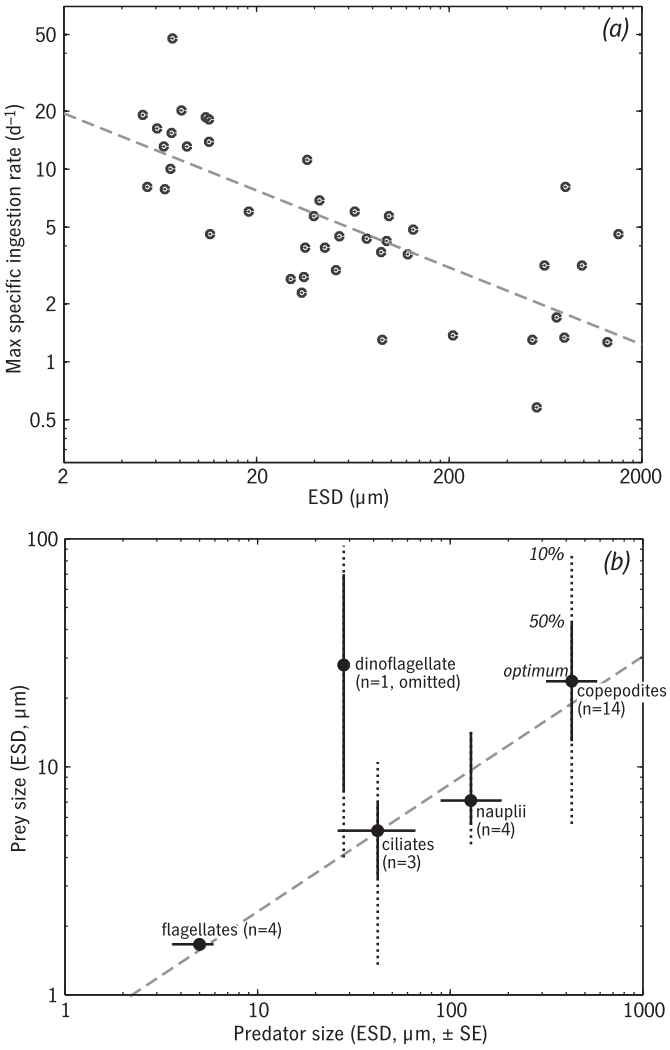

Fig. 2. (a) Allometry of maximum ingestion rate for flagellates, dinoflagellates, ciliates, and copepods, adapted from Hansen et al. (1997). (b) Allometry of prey size preference for several zooplankton taxa, adapted from Hansen et al. (1994). Horizontal bars show the standard deviation of organisms body size, and vertical solid/dotted bars show prey size at which relative grazer preference is 50%/10%. A log-linear regression to all taxa except dinoflagellates (dashed line) was used to parameterize φ, and the width of the preference curves (vertical bars) for ciliates, nauplii, and copepodites was used to choose Δx_{prey}.

Prey size preferences among small flagellates, ciliates, copepod nauplii and copepodites, as surveyed by Hansen et al. (1994), are themselves body size-dependent. The power law (Table 2) is poorly constrained, but no more poorly constrained than that for, e.g., maximum ingestion rate (Fig. 2). Note that it is nevertheless com-

Table 1
Definitions of symbols used in this study, with units where appropriate. μM N = mmol nitrogen m^{-3}.

Symbol	Units	Definition
f_{eg}		Fraction of grazing egested
g_i	d^{-1}	Specific grazing rate for phytoplankton class i
$graz_{ij}$	μM N d^{-1}	Total grazing flux from P_i to Z_j
I_0^j	d^{-1}	Maximum ingestion rate for zooplankton class j
K_s^j	μM N	Prey half-saturation level for zooplankton class j
k_s^i	μM N	Nutrient half-saturation level for phytoplankton class i
m		Phytoplankton mortality, as a fraction of maximum growth rate
N	μM N	Dissolved nutrient stock
n		Number of size classes
P_i	μM N	Phytoplankton biomass in size class i
P_{tot}	μM N	Total phytoplankton biomass
R		Normally distributed random function
r		Stochasticity level
S	μM N d^{-1}	External nutrient supply
x^i_{prey}	μm	Individual size in phytoplankton (prey) class i
$x^j_{prey\ opt}$	μm	Optimum prey size for zooplankton class j
Z_j	μM N	Zooplankton biomass in size class j
Z_{tot}	μM N	Total zooplankton biomass
Δx_{prey}	$\log_{10}$ μm	Prey size tolerance for each grazer
ε		Zooplankton growth efficiency
ζ	$(\mu M\ N)^{-1}\ d^{-1}$	Zooplankton quadratic mortality
μ_0^i	d^{-1}	Maximum uptake/growth rate for phytoplankton class i
φ_{ij}		Preference of grazer Z_j for prey P_i
φ_{ij}^{stoch}		Grazing preferences with stochastic variation included

mon to choose power laws for vital rates using this sort of empirical review but to treat prey size preferences more simply, for mathematical convenience. Note also that the exponent relating optimum prey size to predator body size (Table 2) is far from 1, which is the implicit assumption of models that use a constant predator–prey size ratio. In other words, most small grazers (with a caveat below) eat phytoplankton closer to their own size than large grazers do. Data from the same study were used to choose an empirical, best-fit value for Δx_{prey} of 0.25, based on the observed size selectivity of ciliates, nauplii, and copepodites.

The model implementation discussed here includes 40 equally log-spaced classes of P from 1 to 20 μm, and 40 matching classes of Z from 2.1 to 460 μm. The $x_{prey\ opt}$ power law is used to choose the zooplankton size classes, so that every Z class has its optimal prey size available. It is also important to insure that overall range of P and Z sizes match in this sense, to avoid creating classes of organisms at the small or large ends of the spectrum that are artificially released from grazing pressure or artificially suppressed. A potential elaboration of this model would be to include separate spectra of microzooplankton and mesozooplankton (see Ref. Baird and Suthers, 2007), to allow meaningful inclusion of larger organisms and their life cycles and also to better represent Z predation on Z, which the present model omits.

An important caveat is that heterotrophic dinoflagellates do not follow the $x_{prey\ opt}$ power law: they are relatively large cells that eat phytoplankton of their own size or even larger (Hansen, 1992; Jacobson, 1999). Likewise, autotrophic dinoflagellates fall particularly far below the μ_0 power law (Tang, 1995). Thus even at a broad, functional-group level, this allometric parameterization is far from a complete representation of the evolutionary tradeoffs among the plankton. The allometry used in this study expresses just one essential tradeoff, in which small phytoplankton grow more quickly and scavenge nutrients at low concentrations more effectively than large cells, but are subject to more intense grazing pressure, since their grazers also have higher growth and ingestion rates. In traditional functional-group modeling, it is almost inevitable that this model with its single tradeoff would reduce to two P classes, "small" and "large". However, the results below will demonstrate that resolving trophic complexity creates niches for intermediate, "suboptimal" size classes as well, and changes overall system behavior.

2.3. The monotypic limit

One mathematical consistency check on the model formulation is that in the monotypic limit – that is, the case where all size classes are parameterized identically, or the alternate case where only one size class of P and Z contain any biomass – the model should still behave intelligibly as a three-compartment NPZ model. In either

Table 2
Allometric parameterizations and empirical parameter values used in this study.

Empirical fit	Applicability	Source
$\mu_0^i = (2.6\,d^{-1})\left(\frac{x_i}{1\,\mu m}\right)^{-0.45}$	Phytoplankton 1–100 μm ESD	Tang (1995)
$k_s^i = (0.1\ \mu M\ N)\ \left(\frac{x_i}{1\,\mu m}\right)$	Phytoplankton 5–210 μm ESD	Eppley et al. (1969)
$I_0^j = (26\,d^{-1})\left(\frac{x_j}{1\,\mu m}\right)^{-0.4}$	Flagellates, dinoflagellates, ciliates, copepods	Hansen et al. (1997)
$K_s = 3\ \mu M\ N$	Flagellates, dinoflagellates, ciliates, copepods	Hansen et al. (1997)
$x^j_{prey\,opt} = (0.65\,\mu m)\left(\frac{x^j_{pred}}{1\,\mu m}\right)^{0.56}$	Flagellates, ciliates, nauplii, copepodites	Hansen et al. (1994)
$\Delta x^j_{prey} = 0.25$	Ciliates, nauplii, copepodites	Hansen et al. (1994)

of these limiting cases (identical size classes or a single size class), summing (1)–(3) over i, j yields

$$\frac{dN}{dt} = S - \mu_0 \frac{N}{k_s + N} P_{\text{tot}} \tag{7}$$

$$\frac{dP_{\text{tot}}}{dt} = \left((1-m)\mu_0 \frac{N}{k_s + N} - I_0 \frac{Z_{\text{tot}}}{K_s + P_{\text{tot}}} \right) P_{\text{tot}} \tag{8}$$

$$\frac{dZ_{\text{tot}}}{dt} = \left(\varepsilon I_0 \frac{P_{\text{tot}}}{K_s + P_{\text{tot}}} - \zeta Z_{\text{tot}} \right) Z_{\text{tot}} \tag{9}$$

The one difficulty is the normalization of φ, which cannot be made to satisfy both these monotypic limits simultaneously. As written in (5), φ is normalized correctly for the single-size class limit. In the identical-size-class limit – as is true in general unless $P_i(x)$ and φ_{ij} are specially constructed – the fact that $\Sigma_i(\varphi_{ij} P_i) \neq P_{\text{tot}}$ means that the effective prey half-saturation level for the community as a whole is somewhat different from K_s. (This can be shown by summing (4) over i and writing the result in terms of P_{tot} and an effective half-saturation, which can then be solved for algebraically: see Ref. Gentleman et al. (2003) for further discussion of this normalization issue.) In other words, K_s should be thought of as merely a *scale* for the prey half-saturation, which depends on the prey biomass distribution and thus changes over time and among cases.

Eqs. (7)–(9) can be used to choose a biologically reasonable value for the mortality parameter ζ. For a long-term equilibrium to be possible when $P_{\text{tot}} \approx K_s$, it is necessary that:

$$\zeta \approx \frac{\varepsilon I_0^2}{4\mu_0 K_s} \tag{10}$$

or, for the median values of I_0^j and μ_0^i along the size spectrum, $\zeta \approx 1\ \mu\text{M}^{-1}\text{d}^{-1}$. This is the value used for the base-case experiment below.

2.4. Code implementation

The source code and a graphical interface to this model are available online at http://faculty.washington.edu/banasn/models/astrocat. This model implementation, which includes both the model itself and an interactive visualization system, is written in Java using the Processing toolkit (http://www.processing.org). It has been designed to encourage adaptation by others, not just to investigate planktonic diversity as discussed in this paper, but also as a convenient means for nonspecialists to implement and investigate any model in the NPZ family (or stock-flux models in general). A model running in this visualizer consists of an "Ecosystem" code object linked to an "Environment" object which handles timestepping (in this version, a first-order implicit scheme) and also provides a means for constructing a spatially resolved domain more elaborate than the zero-dimensional box used here. The "Ecosystem" object contains lists of "StateVariables", "Fluxes" and "FreeParameters", each definable in one line of code, and a method (which runs on each timestep) in which formulas for the Fluxes are given. Thus Eqs. (1)–(3) are represented in code as a list of the individual fluxes that constitute each balance, with exchanges between compartments and tracer conservation handled at a deeper, more utility-like level of the code. This makes modification and replacement of the biological model itself much easier. Basic NPZ and NPZD (nutrient–phytoplankton–zooplankton–detritus) models are included in the code package as templates for other applications. When run as a desktop application, this visualizer also allows one to save results for quantitative analysis in the NetCDF file format. Scripts that replicate all model experiments shown in this paper are also included.

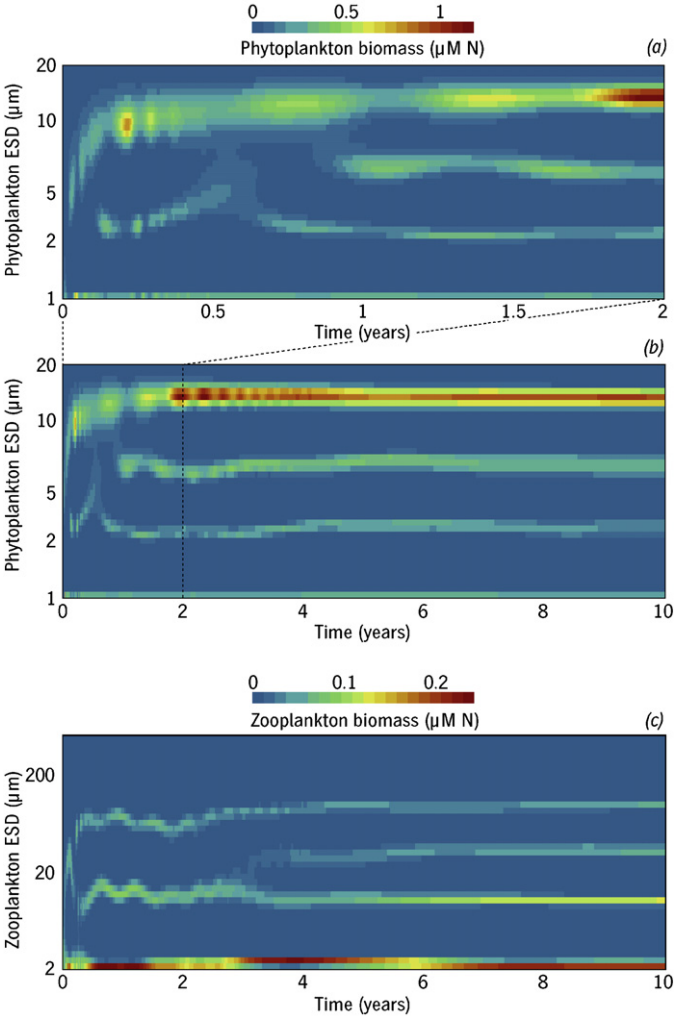

Fig. 3. Biomass under steady nutrient forcing in the model base case. (a and b) Phytoplankton biomass by size class over 2 and 10 years of model time evolution. (c) Ten years of zooplankton time evolution.

3. Results

3.1. Behavior under steady forcing

3.1.1. Structure of the size spectrum

To explore the basic dynamics of the ASTroCAT model, I will begin with a set of experiments under steady nutrient forcing. A range of nutrient-supply levels from 0.06 to 4 $\mu\text{M}\,\text{d}^{-1}$ was tested. This maximum value is high but still physically realistic: 4 $\mu\text{M}\,\text{d}^{-1}$ throughout a 20 m surface layer is equivalent to 0.9 $\mu\text{mol}\,\text{m}^{-2}\,\text{s}^{-1}$, at the nominal high end of turbulent nitrate fluxes measured by Hales et al. (2005) on the Oregon inner shelf, an active upwelling zone. I will use $S = 1\ \mu\text{M}\,\text{d}^{-1}$ as the base case.

Time series of P and Z biomass by size class are shown in Fig. 3 for a 10 year run of the base case, along with time series of P_{tot} and Z_{tot}. Two features of the solution are immediately apparent. First, biomass is highly clustered into certain sets of size classes, rather than forming a continuous size spectrum. The slope of the planktonic biomass size spectrum has frequently been invoked as a key metric of community structure and function (Sheldon et al., 1972; Zhou and Huntley, 1997), and so the nonmonotonicity of these results is striking. At the same time, peaks and valleys along the size spectrum have also been frequently observed in real plankton populations (Chisholm, 1992; Schartau et al., 2010), particularly in

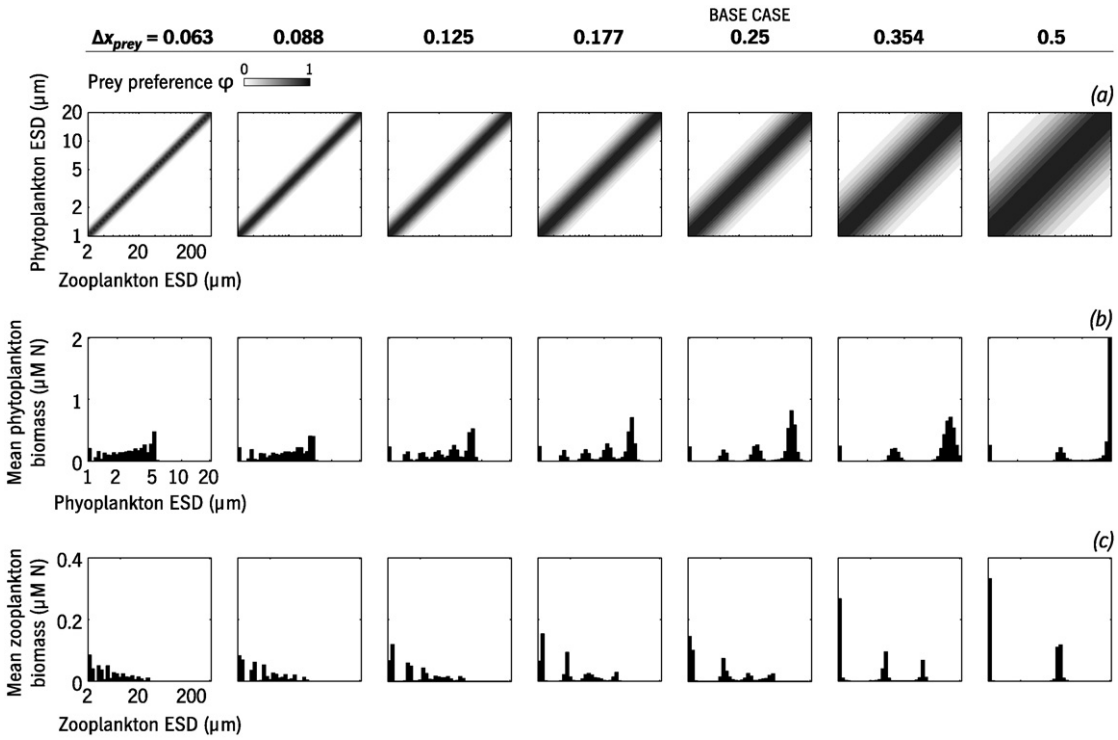

Fig. 4. Effect of grazer selectivity, i.e., the width Δx_{prey} of the prey preference function φ (a), on time–mean biomass size spectra for phytoplankton (b) and zooplankton (c). The model base case, with Δx_{prey} chosen from general laboratory data (Fig. 2b), is labeled.

enriched or naturally nutrient-rich systems (Cavender-Bares et al., 2001). It is common to attribute these peaks and valleys to transient trophic interactions (references above), and indeed, in this model, the size clustering appears to be a direct result of the structure given to the prey preferences. Even when all other variation among size classes besides φ_{ij} is turned off (not shown), the P and Z biomass spectra show this clustering.

A set of experiments in which Δx_{prey} was varied 8-fold around the base case (Fig. 4) demonstrates that the spacing of biomass–spectrum peaks is controlled by the grazers' size selectivity. When Z classes are highly specialized in their prey (Δx_{prey} small), the biomass spectra approach continuous distributions, while generalist grazers (Δx_{prey} large) yield spectra with only two or three peaks. One might expect that a more complicated model, in which a wider variety of evolutionary strategies among the phytoplankton were represented, would yield spectra with more classes of "winners" in them and thus somewhat more continuous spectra; likewise for a model in which physical variability were allowed to realistically perturb the plankton community on a range of timescales.

The second notable feature of the base-case biomass size spectrum (Fig. 3) is its time-dependence. The system does not reach steady state, even in qualitative terms, for several years: the P and Z communities shift from 3- to 4-peak spectra after 1 and 4 years, respectively (Fig. 3a and c). Oscillatory tradeoffs between size classes occur with periods from days to years, despite the fact that even the largest and slowest-growing organisms included have vital rates on the order of $1\,\text{d}^{-1}$. This system does not appear to be chaotic, tending as it does to an uncomplicated steady state: when the model is run for a further 90 years (not shown), no new changes in qualitative behavior appear. Nevertheless, in a pragmatic sense – in terms of the model's predictive power when applied to real systems – this long-term time dependence has implications similar to the chaotic behavior observed in other ecosystem models (Baird, 2010; Hastings and Powell, 1991; May, 1976) as well as in living planktonic systems (Benincà et al., 2008). These implications are considered further below, in the context of realistically time-varying nutrient forcing. First, I will use this simpler, steady-forcing case to examine mechanistic relationships between growth, grazing, and community structure and function.

3.1.2. Response to nutrient supply and grazing pressure

A set of cases varying the one bottom-up control in the model, nutrient supply S, and another set varying the one top-down control, higher mortality ζ, are shown in Fig. 5. The time–mean P biomass spectrum is used as one metric of the system response, along with two measures of ecosystem function: a nutrient-limitation metric for each P size class $k_s^i\,(k_s^i+N)^{-1}$ and a grazing-limitation metric for each size class g_i/μ_i, where g_i is the effective grazing rate

$$g_i \equiv \frac{1}{P_i}\sum_j graz_{ij} \tag{11}$$

When this nutrient limitation metric equals 0, nutrients are saturating, and when it equals 1, they are fully exhausted. When this grazing limitation metric equals 0, grazing is completely absent, and when it equals 1, grazing balances primary production and population growth stops (although to be more precise, because of the "other mortality" term in (1), population growth is slightly negative at this point).

As S is increased, the abundance of large phytoplankton increases (Fig. 5a). This is an important test of the realism of the model, shown more summarily in Fig. 6. At low nutrient-supply levels, small phytoplankton dominate the community, while as nutrient supply increases, the small-phytoplankton population responds relatively weakly while the >5 μm fraction of the phytoplankton population increases dramatically. This accords with observations from many high- and variable-nutrient-supply systems (Chisholm, 1992). Increasing S also moves the system,as one

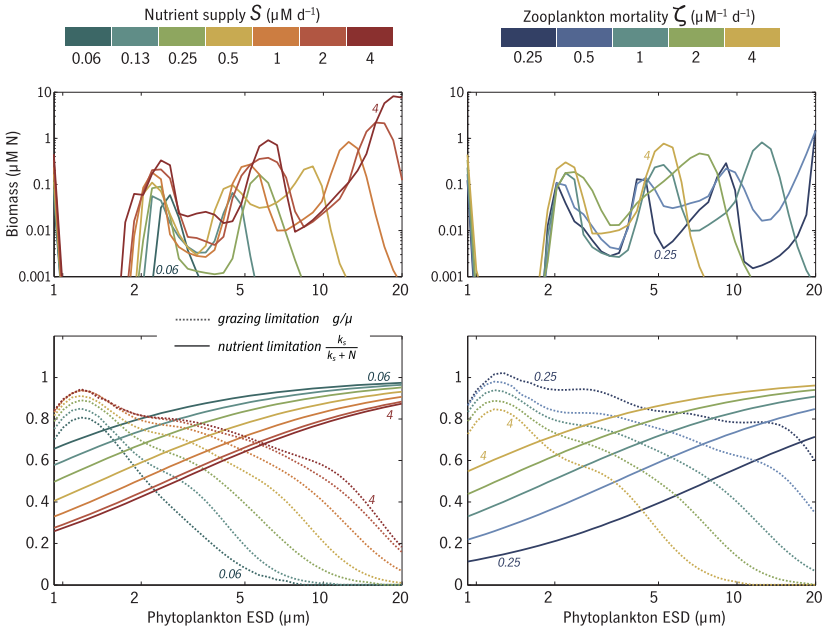

Fig. 5. Effect of varying external nutrient supply S and higher predation on zooplankton ζ on mean phytoplankton biomass spectra (top) and metrics of grazing limitation and nutrient limitation (bottom) for each size class.

would expect, away from nutrient limitation and toward grazing limitation, that is, top-down control (Fig. 5c). Increasing ζ has the opposite effect (Fig. 5d), shifting the system toward bottom-up control, via a trophic cascade in which grazing is suppressed by higher predation.

3.1.3. Effect of stochastic prey preference

Since the selectivity of individual grazers appears to be important (Fig. 4), it is worth asking to what extent the patterns discussed above are artifacts of the relative lack of variation from one grazer to the next in this smooth, allometric parameterization. The broad-scale allometric variations discussed so far might be taken to represent functional-group-level diversity, in a mathematically simple way. Next I will discuss the effect of adding stochasticity to the grazing preferences (Eq. (6)), meant to represent species-level diversity. Microzooplankton can be extremely selective in their feeding (Burkhill et al., 1987; Flynn et al., 1996; Stoecker et al., 1981), even among nearly identical prey species (Olson et al., 2008), in ways that size-based prey preferences – or indeed, any parameterization short of listing individual species – are unable to capture. Adding stochastic noise to φ_{ij} is a crude mathematical representation of this diversity, which provides a test of the model's sensitivity to these unparameterizable fine-scale preferences.

Eight sets of stochastic noise (**R** in Eq. (6)) were constructed and incorporated into the prey preferences at a range of values of the stochasticity parameter r. Phytoplankton biomass by size class over time, as in Fig. 3, is shown in Fig. 7 for one example case out of these eight. At $r = 1$, the temporal variability of the system increases dramatically, with large-magnitude blooms of individual size classes taking place on timescales from a few days to hundreds of days. The amplitude of this temporal variability shows no obvious trend over the 10 year model run, in contrast to the asymptotic behavior of the nonstochastic $r = 0$ case (Figs. 3b and 7a). The clustering into four peaks along the size spectrum seen in the steady case is also disrupted. Signs of all these behaviors, particularly the last, are also apparent at a much lower level of stochastic variation ($r = 0.25$, Fig. 7b).

At $r = 0.25$, despite the disruption of the smoothly clustered size spectrum, there is no significant change in mean total biomass relative to the base case (mean $P_{tot} = 3.7 \pm 0.3$ μM N for the ensemble of 8 cases, compared with 3.8 μM N for $r = 0$). Likewise, the nutrient-limitation and grazing-limitation metrics shown in Fig. 5 only shift by 3% to 11%, respectively. Under more extreme stochastic variation ($r = 1$), the shifts in these mean metrics do become significant (e.g., mean $P_{tot} = 10 \pm 2$ μM N), but it appears that overall ecosystem function is insensitive to small-to-moderate ($r = 0.25$) variation in the details of the prey preferences.

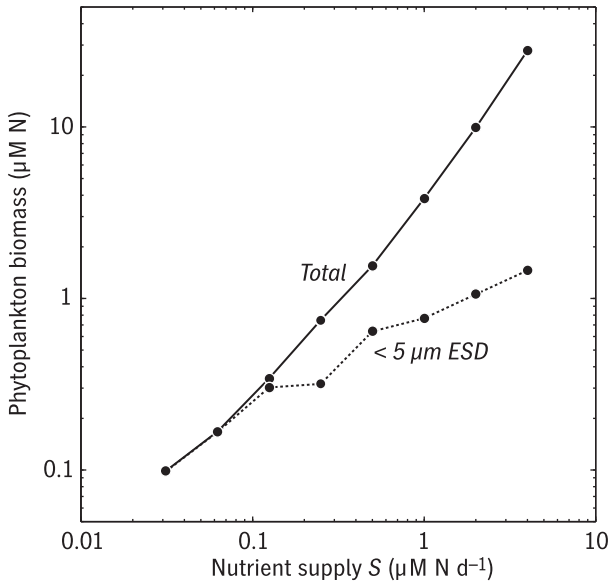

Fig. 6. Relationship between total phytoplankton biomass, biomass in the <5 μm size range, and nutrient supply, demonstrating that community shifts sensibly from domination by small cells to domination by large cells over a realistic range of nutrient supply levels.

3.1.4. Diversity patterns

This last result confirms the common rule of thumb that while functional-group-level diversity among the plankton is crucial to marine ecosystem dynamics, the noise introduced by species-level

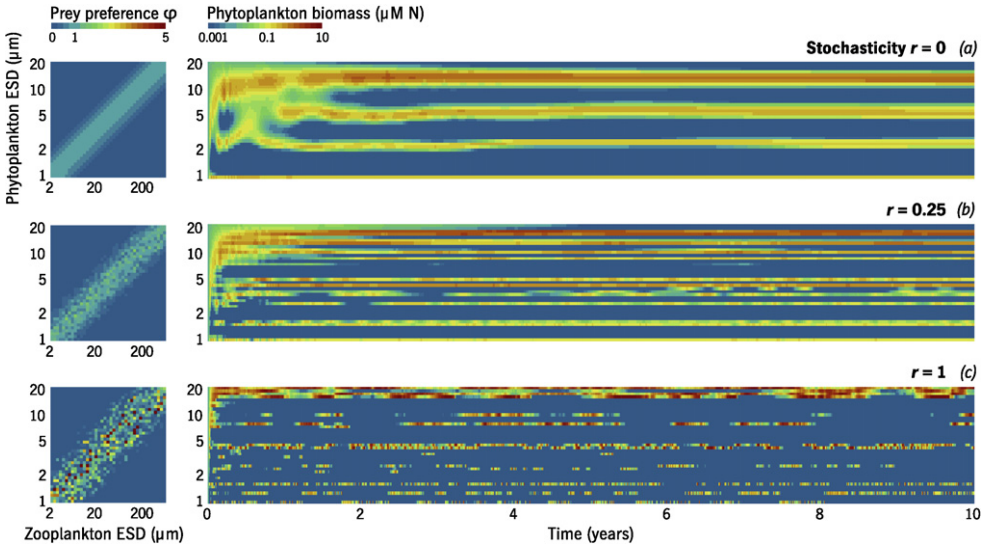

Fig. 7. Matrix of prey preferences φ and ESD-versus-time diagrams of phytoplankton biomass for an example case drawn from an ensemble of experiments adding fine-scale, stochastic noise to the prey preferences. Results are shown for three values of the stochasticity parameter r (see Eq. (6)), with the random noise function **R** held constant. The $r = 0$ case (a) is identical to the model base case shown in Fig. 3, although here biomass is plotted on a log rather than linear scale, to better show the intense transient blooms that develop as r is increased (b and c).

variation can largely be averaged away in a broad-scale description of a system. Nevertheless, a model system like ASTroCAT raises the possibility of investigating or predicting patterns of variation on the species level, rather than simply averaging them away. The relationship between ecosystem diversity and total biomass is shown in Fig. 8. Diversity is quantified here using the Shannon evenness

$$-\frac{1}{n}\sum_{i}\frac{P_i/P_{\text{tot}}}{\ln(P_i/P_{\text{tot}})} \tag{12}$$

where $n = 40$ is the number of species or size classes. For each stochastic case with $r = 1$, as well as for the nonstochastic base case, nutrient supply was varied as in Figs. 5 and 6, and time-mean biomass and evenness calculated for both P and Z. Total phytoplankton biomass varies parabolically with evenness (Fig. 8a), with or without stochastic variation in the prey preferences. That is, as biomass increases with increasing nutrient supply (a monotonic relationship in all cases), diversity is relatively low when biomass is either very low or very high. This replicates the result of Irigoien et al. (2004), who concluded that planktonic biomass and diversity had a parabolic relationship in general based on a broad compilation of field observations. Irigoien et al. (2004) found this to be true for both phytoplankton and zooplankton, whereas in this model it true for phytoplankton only. It is possible that the diversity pattern for zooplankton in the model would change if the next level of trophic interactions were explicitly resolved.

3.2. Behavior under time-varying forcing

The experiments described so far under steady nutrient forcing show that internal variability in this model ecosystem (predator–prey and competitive interactions) give rise to long-lived transients on timescales up to 1–2 years. This raises the possibility of interaction between internal variability and variability in external forcing, not just on bloom timescales but on seasonal or interannual scales as well. In future work, in a more realistic testbed, this could be explored by driving ASTroCAT with realistically time-variable forcing and testing it against actual observations. As a first step in this direction, I conducted a set of model runs in which the nutrient supply was varied in a sinusoidal seasonal cycle, from 0 to 1 μM d^{-1}. This scenario is meant to represent the annual cycle in a temperate upwelling zone like

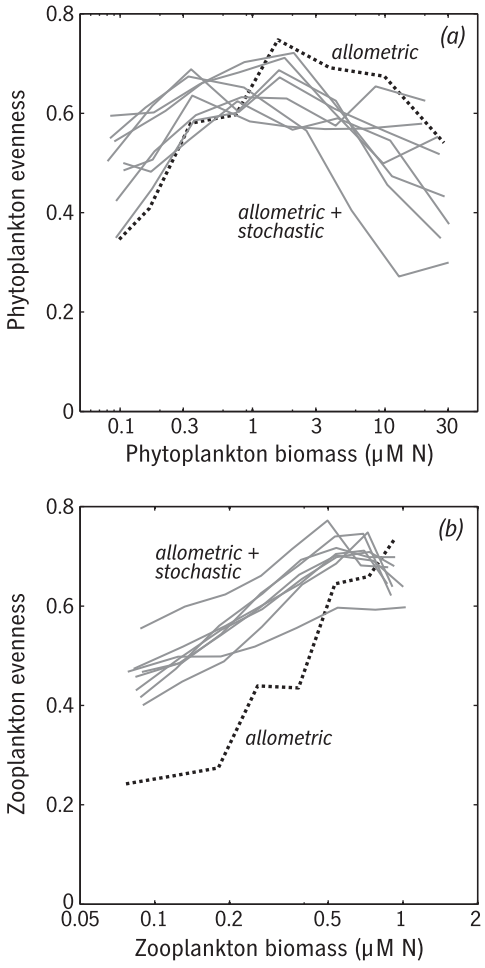

Fig. 8. Shannon evenness (Eq. (12)) for phytoplankton and zooplankton as a function of biomass, as nutrient supply is varied in the allometric base case (dotted line) and an ensemble of stochasticity-adding cases (solid gray lines). In all cases, the relationship between phytoplankton diversity and biomass is parabolic, but the relationship between zooplankton diversity and biomass is close to monotonic.

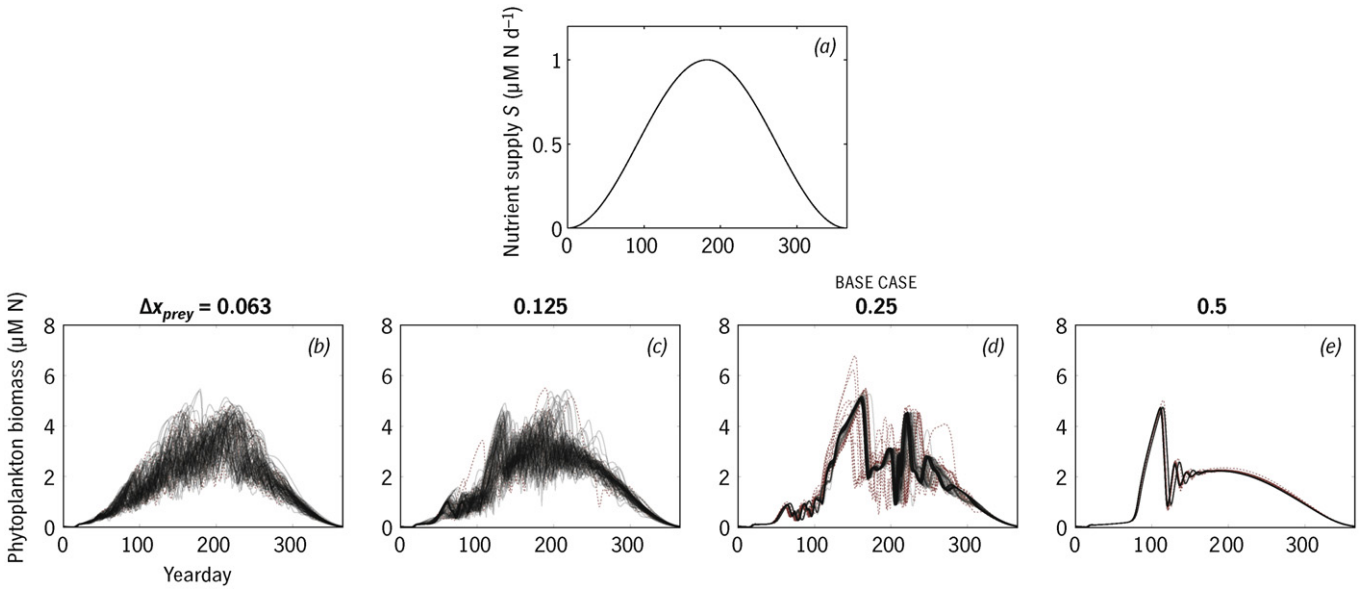

Fig. 9. Annual-cycle experiments in which a sinusoidal pattern of nutrient supply (a) is repeated exactly for 100 years, and the resulting 100 annual cycles of phytoplankton biomass superimposed as a function of yearday, for each of four experiments at varying levels of grazer selectivity Δx_{prey} (b–e). The initial 20 years are plotted as thin red dotted lines, years 21–100 as thin black solid lines.

the California Current System (CCS), although in the real CCS light rather than nutrients is generally limiting in winter. (Better realism would require a less minimalist testbed.) These runs were 100.5 years long, beginning in mid-summer – the first 6 months are discarded as spinup – and they can be thought of as 100 sequential realizations of the annual cycle, in which the only difference between realizations is the biomass initial condition, the seed stock left after the previous year's summer bloom dies back in winter.

Results are shown in Fig. 9b for a range of prey size tolerances Δx_{prey}. The initial 20 years of each run are shown as red dotted

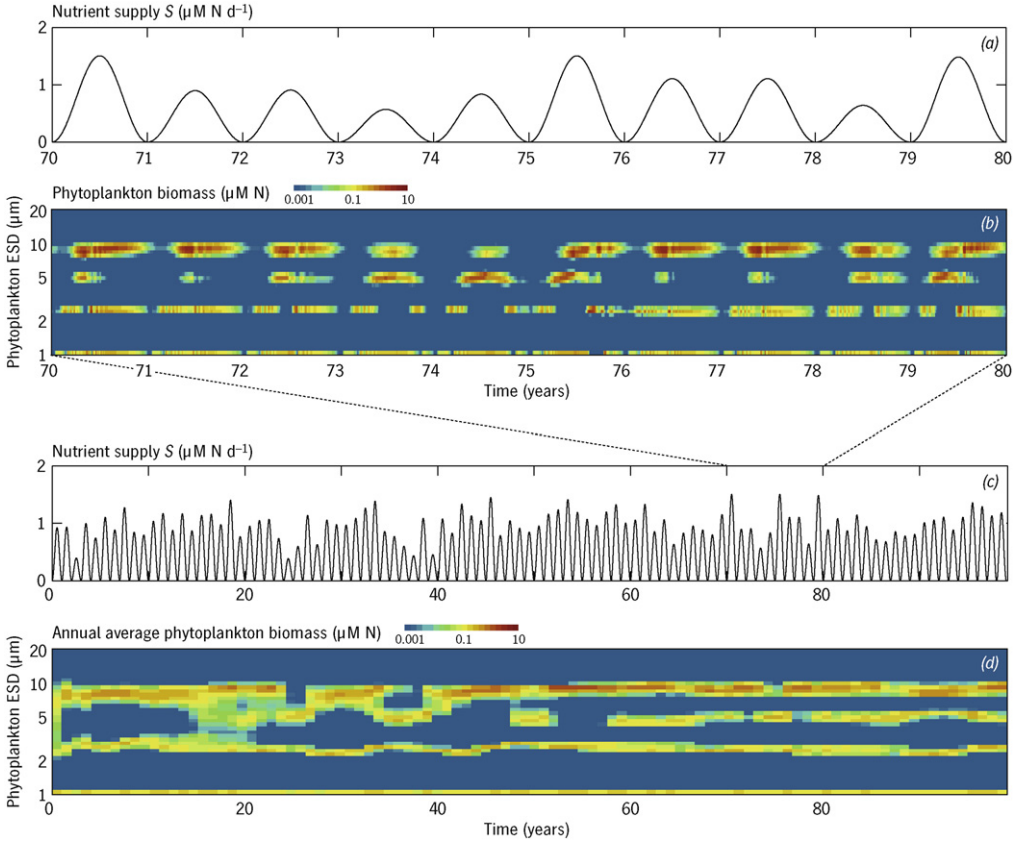

Fig. 10. Nutrient supply (a and c) and phytoplankton biomass by size class (b and d) over a 100 year model run in which an annual cycle of nutrient supply (as in Fig. 9) was modulated by a normally distributed random function to produce interannual variation (c). A ten year slice of this model run is magnified in (a and b). Nutrient forcing and annual-mean biomass for the full model run are shown in (c and d).

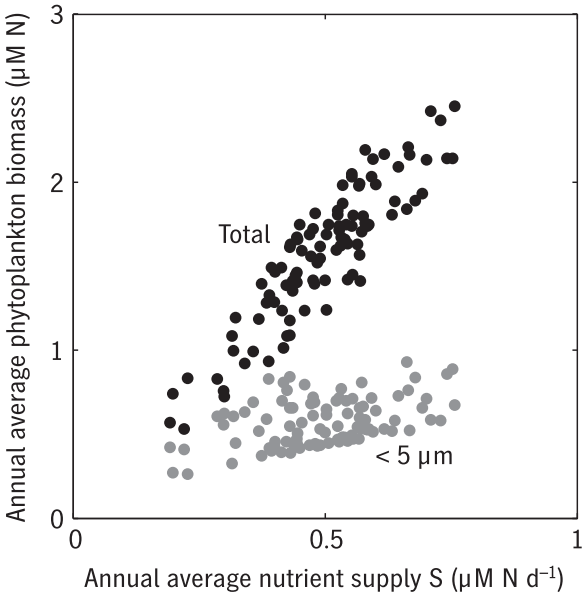

Fig. 11. Annual-mean phytoplankton biomass as a function of annual-mean nutrient supply, for the model run shown in Fig. 10c and d. Total biomass and biomass in the <5 μm range are shown: compare Fig. 6.

lines, so that initial transients can be distinguished from long-term behavior. When Δx_{prey} is small and grazers highly selective (compare Fig. 4), the mean annual cycle of biomass follows the sinusoidal pattern of the forcing, although there is also persistent bloom-timescale variation of approximately a factor of two throughout the model run. In contrast, at very large Δx_{prey}, the 100-year time series quickly collapses to a fixed annual cycle without significant year-to-year variation. This cycle is likewise approximately sinusoidal, following the forcing time series, except for a large and repeatable spring bloom. At the medium value of Δx_{prey} that represents the empirical base case, there is, as in the large Δx_{prey} case, a fixed annual cycle in the model's long-term behavior. This cycle, however, is much more complicated than the nutrient forcing function, with a number of spring and mid-summer blooms superimposed on the basic sinusoid. In addition, this model case shows strong, long-lived transients superimposed on this long-term solution: variation in bloom amplitude up to a factor of two, persisting 10–20 years into the simulation (red dotted lines).

This decades-long ringing of the model's initial condition suggests the hypothesis that if forcing were to vary on the same interannual or decadal scale, a steady state might never be achieved, or at least be delayed. To test this, I conducted another set of 100-year runs in which the amplitude of each year's peak nutrient supply varied randomly around the mean of 1 μM d^{-1}, in a normal distribution with std dev 0.25 μM d^{-1}. A sample decade (years 70–80) in the base-case simulation is shown in Fig. 10a and b, with annual averages of S and P_i for the full run shown in Fig. 10c and d. The correlation between annual-mean S and annual-mean P biomass is shown in Fig. 11, for total biomass and the <5 μm size fraction, as in Fig. 6. Biomass is significantly correlated with nutrient supply on this timescale, but there is also substantial interannual variance unexplained by this relationship as well ($r^2 = 0.8$, not 1). Since nutrient supply is the only external factor varying between years, the unexplained variance in this correlation can be taken as a quantification of the inherent unpredictability of the ecosystem (in a pragmatic sense: this system may or may not be chaotic in the mathematical sense).

The 100-year interannual-variation experiment was repeated for a range of values of Δx_{prey}, to examine the effect of grazer selectivity and thus food-web complexity on system predictability (Fig. 12a). In general, as selectivity decreases and complexity increases, the system's biomass response to nutrient forcing becomes more unpredictable, with up to 40% of interannual variance not explained by any external factor (i.e., $r^2 = 0.6$). Note that this monotonic trend ends abruptly at $\Delta x_{\text{prey}} = 0.421$, when the mean P biomass spectrum switches from three distinct peaks to two, similar to the progression shown in Fig. 4b for the steady-forcing case. The same experiment was repeated using the base-case value of Δx_{prey} but varying the number of P, Z size classes n from 2 to 80 (Fig. 12b). The $n = 2$ case represents a simple division into "small" and "large" phytoplankton, which would, as discussed above, be a natural way to represent the biology included in ASTroCAT in a functional-group-style as opposed to size-spectral NPZ model. At this low- n limit, $r^2 \approx 1$, meaning that annual-mean S is almost a perfect predictor of annual-mean P_{tot}. Between $n = 4$ and $n = 6$, the model's behavior switches abruptly to a regime in which $r^2 \approx 0.8$, including the base case. This suggests that the inherent unpredictability of this system results from internal dynamics that require a certain level of diversity resolution to appear.

4. Discussion and conclusions

4.1. Summary

To summarize, the model described above extends recent work in size-spectral plankton modeling by parameterizing zooplankton feeding preferences as realistically and empirically as can be done in allometric terms (Fig. 2b), by analogy with common practice for treating vital rates (e.g., Fig. 2a). Experiments were also conducted adding stochastic, fine-scale, "species-specific" variation to these allometric prey preferences. The result is a model ecosystem whose behavior approaches the complication of real data, both for better and for worse. By "for worse" I mean the occurrence of strong and very long-lived transients, whose significance I will discuss further below. By "for better" I mean the emergence of nontrivial mean patterns of community structure, which suggest quantitative, testable links (i) between the waviness of the size spectrum and grazer selectivity (Fig. 3), and (ii) between phytoplankton diversity and biomass (Fig. 8).

A set of annual-cycle and interannual-variability experiments (Figs. 9 and 10) show a complicated relationship between food-web complexity (here represented by the width of each grazer's prey size tolerance) and the predictability of the ecosystem under slow changes in nutrient supply. I use "predictability" here in the pragmatic sense of "allowing one to model ecosystem response to external forcing based on a simple rule, such as a linear regression". It is necessary to distinguish between multiple timescales of predictability to summarize the ASTroCAT results.

On the *bloom* timescale, unpredictability *decreases* with increasing food-web complexity. That is, for specialist grazers (Δx_{prey} small: Fig. 9b), the time evolution of phytoplankton biomass over a single growing season is full of factor-of-two variation on timescales of days to weeks, not forced by any change in nutrient supply other than the annual cycle. For generalist grazers (Δx_{prey} large: Fig. 9e), the population's time evolution over one season is very smooth. This pattern confirms the results of Baird and Suthers (2010), who found that increasing structural complexity in a different size-spectral plankton model also resulted in reduced growth of initial-condition perturbations over a few hundred days. On the *interannual* scale, however, the opposite pattern occurs. Unpredictability *increases* with increasing food-web complexity, up to a high threshhold near $\Delta x_{\text{prey}} \approx 0.4$, where community structure and time-evolution suddenly simplify. The correlation between annual-average nutrient supply and P biomass over a range of interannual-variation experiments (Fig. 12) shows

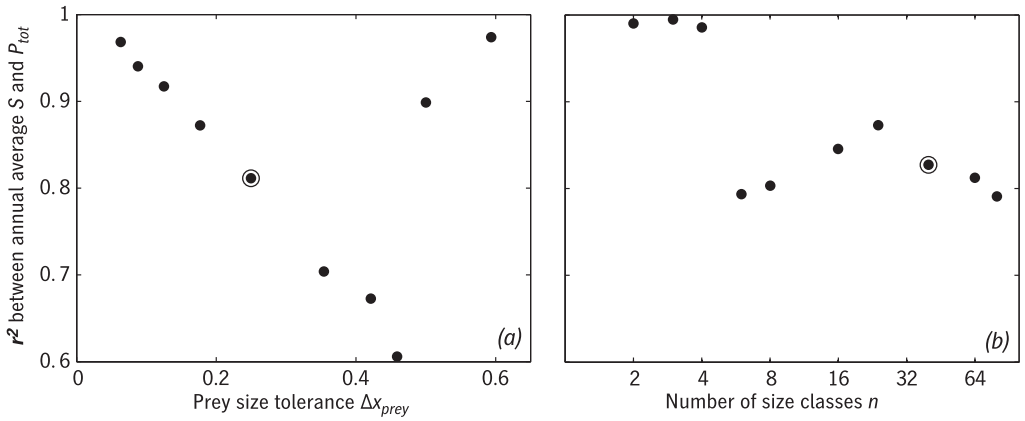

Fig. 12. Correlation r^2 between annual-mean nutrient supply and annual-mean phytoplankton biomass, as grazer selectivity (a) and number of size classes (b) are varied around the model base case shown in Figs. 10 and 11 (circled points). High values of r^2 indicate a simple, predictive relationship between bottom-up forcing and ecosystem response; low values indicate the partial confounding of this relationship by internal variability.

this most clearly, but the magnitude and duration of initial transients in the annual-cycle cases (Fig. 9b–e, red dotted lines) show the same behavior.

The diversity of ecosystem behaviors in this parametric landscape is strong motivation for treating trophic interactions in plankton models with the same care and empiricism as phytoplankton physiology and growth. Gentleman et al. (2003) highlights the wealth of biological implications that go along with any choice of functional form for grazing, most of them probably unintended and possibly pathological. The focus in this study on the shape of the prey preferences is intended as a complement. Further theoretical work on the relationship between grazing, stability, and diversity needs to consider functional responses and prey preferences simultaneously, along the lines of Post et al. (2000).

4.2. Implications for ecosystem prediction

What does the emergent unpredictability of models like ASTroCAT or that of Baird (2010) mean for the practical goal of numerical ecosystem forecasting? An analogy with circulation and climate modeling is useful. Hawkins and Sutton (2010) divide uncertainty in regional climate models into (i) internal variability, (ii) model uncertainty, which includes both parameter uncertainty and structural uncertainty related to model design, and (iii) uncertainty in forcing scenarios. They find that all three of these categories can be dominant at some timescale of prediction. In biogeochemical modeling, model uncertainty has received the most attention (Fennel et al., 2001; Friedrichs et al., 2007; Fulton et al., 2003, 2004). There is no a priori reason, however, to think that internal variability is less important to ecosystem prediction than it is to the regional climate models described by Hawkins and Sutton (2010). In climate modeling, this internal variability consists of free oscillating modes like ENSO, the Pacific Decadal Oscillation, the North Atlantic Oscillation, and so on. In atmospheric modeling, it can be thought of as synoptic-scale weather systems; in ocean circulation modeling, it consists of eddies and unstable jets. In biogeochemical modeling, it consists largely of transient blooms and predator–prey oscillations, "ecosystem weather", and in general it is suppressed in order to make bottom-up linkages clear and clean.

This suppression of internal variability can happen in a number of ways. It is a natural consequence of omitting planktonic diversity, and thus happens by default in simple NPZ-type models, as in ASTroCAT for $n \leq 4$ (Fig. 12b). It happens as well in models where phytoplankton diversity is resolved but predator diversity is omitted or minimal (Bruggeman and Kooijman, 2007; Follows et al., 2007). In some cases it is very much by design: Armstrong (2003) presents a method for constructing the grazer field in a size-spectral model specifically to eliminate predator–prey oscillations, treating these oscillations, as is common, as instabilities analogous to the purely numerical errors that arise from a poor discretization or timestepping scheme.

For many large-scale biogeochemical applications, these approaches are appropriate and powerful. In other contexts, however, it may be better to view predator–prey oscillations in plankton models not as errors at all, but rather as idealizations of real and potentially important internal variability, as suggested by the analogies above. In ocean circulation modeling, one does not intentionally suppress eddies, but rather works to resolve them, and then averages. Likewise, when a global climate model produces a century-scale projection of future change, that projection also contains daily weather and free interannual oscillations; the statistics of this short-term internal variability are important metrics of the model results and can also be used as checks on the model's mechanistic validity. ASTroCAT is an experiment in treating the transients associated with trophic complexity in the same terms, as real dynamics to resolve and quantify, rather than artifacts to suppress.

This shift in perspective opens up new possibilities in ecosystem forecasting. First, it makes possible a new kind of ensemble forecasting with analogs in weather and climate modeling (Bracco et al., 2004; Di Lorenzo et al., 2010; Tebaldi and Knutti, 2007), in which without any manipulation of parameter values, initial conditions are varied slightly among multiple realizations in order to reveal and isolate chaotic internal variability. The interannual-variability experiments described above (Fig. 11) suggest how this approach could be used to distinguish the "bottom-up-deterministic" portion of the ecosystem response from inherently unpredictable trophic effects. This approach allows one to place confidence limits on a model result and define a fundamental limit to system predictability (Huisman and Weissing, 2001) on a given timescale.

The second opportunity that arises from resolving rather than suppressing trophic complexity is an expanded ability to treat diversity patterns as a dynamic part of the solution (Fig. 8). As a point of comparison, consider the trait-based model of Bruggeman and Kooijman (2007), which yields a phytoplankton community that always responds optimally to nutrient and light conditions, but which, as a result of its optimality, cannot simulate or explain coexistence Huisman and Weissing (1999) and Hutchinson (1961). Region- or problem-specific models built with an alternative logic similar to ASTroCAT, in which optimality is probably never achieved in any realistic, time-variable forcing scenario, would allow one to quantitatively test hypotheses concerning

coexistence, species persistence, and predictability of individual species within a population, along the lines of Litchman et al. (2009), Weitz and Levin (2006) and Williams (2008). These applications would be most relevant to problems where "ecosystem weather" is of central concern, like controls on and predictability of harmful algal blooms.

Acknowledgements

This work was supported by the Coastal Ocean Program of the National Oceanic and Atmospheric Administration (NA09NOS4780180) and the National Science Foundation (OCE 0239089, OCE 0238347, OCE 0942675). This is contribution #645 of the NOAA ECOHAB (Ecology of Harmful Algal Blooms) program, #53 of the NSF RISE (River Influences on Shelf Ecosystems) program, and #5 of the NSF/NOAA PNWTOX (Pacific Northwest Toxins) program. The contents are solely the responsibility of the author and do not necessarily represent the official views of the supporting agencies. Many thanks to an anonymous reviewer, Mark Baird, Peter Franks, Raphe Kudela, Jamie Pierson, Andy Leising, Mick Follows, and Evelyn Lessard for their insights and suggestions.

References

Armstrong, R.A., 2003. A hybrid spectral representation of phytoplankton growth and zooplankton response: the control rod model of planktonic interaction. Deep-Sea Research II 50, 2895–2916.

Baird, M.E., 2010. Limits to prediction in a size-resolved pelagic ecosystem model. Journal of Plankton Research 32, 1131–1146.

Baird, M.E., Suthers, I.M., 2007. A size-resolved pelagic ecosystem model. Ecological Modelling 203, 185–203.

Baird, M.E., Suthers, I.M., 2010. Increasing model structural complexity inhibits the growth of initial condition errors. Ecological Complexity 7, 478–486.

Benincà, E., Huisman, J., Heerkloss, R., Jöhnk, K.D., Branco, P., van Nes, E.H., Scheffer, M., Ellner, S.P., 2008. Chaos in a long-term experiment with a plankton community. Nature 451, 822–825.

Bracco, A., Kucharski, F., Kallummal, R., Molteni, F., 2004. Internal variability, external forcing and climate trends in multi-decadal AGCM ensembles. Climate Dynamics 23, 659–678.

Bruggeman, J, Kooijman, S.A.L.M., 2007. A biodiversity-inspired approach to aquatic ecosystem modeling. Limnology and Oceanography 52, 1533–1544.

Burkhill, P.H., Mantoura, R.F.C., Llewellyn, C.A., Owens, N.J.P., 1987. Microzooplankton grazing and selectivity of phytoplankton in coastal waters. Marine Biology 93, 581–590.

Cavender-Bares, K.K., Rinaldo, A., Chisholm, S., 2001. Microbial size spectra from natural and nutrient enriched ecosystems. Limnology and Oceanography 46, 778–789.

Chen, X., Cohen, J.E., 2001. Transient dynamics and food-web complexity in the Lotka–Volterra cascade model. Proceedings of the Royal Society B 268, 869–877.

Chisholm, S.W., 1992. Phytoplankton size. In: Falkowski, P.G., Woodhead, A.D. (Eds.), Primary Productivity and Biogeochemical Cycles in the Sea. Plenum Press, New York, pp. 213–237.

Di Lorenzo, E., Cobb, K.M., Furtado, J.C., Schneider, N., Anderson, B.T., Bracco, A., Alexander, M.A., Vimont, D.J., 2010. Central Pacific El Niño and decadal climate change in the North Pacific Ocean. Nature Geoscience 3, 762–765.

Edwards, A.M., Yool, A., 2000. The role of higher predation in plankton population models. Journal of Plankton Research 22, 1085–1112.

Eppley, R.W., Rogers, J.N., McCarthy, J.J., 1969. Half-saturation constants for uptake of nitrate and ammonium by marine phytoplankton. Limnology and Oceanography 14, 912–920.

Fennel, K., Losch, M., Schröter, J., Wenzel, M., 2001. Testing a marine ecosystem model: sensitivity analysis and parameter optimization. Journal of Marine Systems 28, 45–63.

Flynn, K.J., Davidson, K., Cunningham, A., 1996. Prey selection and rejection by a microflagellate; implications for the study and operation of microbial food webs. Journal of Experimental Marine Biology 196, 357–372.

Follows, M.J., Dutkiewicz, S., Grant, S., Chisholm, S.W., 2007. Emergent biogeography of microbial communities in a model ocean. Science 315, 1843–1846.

Franks, P.J.S., 2002. NPZ models of plankton dynamics: their construction, coupling to physics, and application. Journal of Oceanography 58, 379–387.

Friedrichs, M.A.M., et al., 2007. Assessment of skill and portability in regional marine biogeochemical models: role of multiple planktonic groups. Journal of Geophysical Research 112 (C08001).

Fuchs, H.L., Franks, P.J.S., 2010. Plankton community properties determined by nutrients and size-selective feeding. Marine Ecology Progress Series 413, 1–15.

Fulton, E.A., Smith, A.D.M., Johnson, C.R., 2003. Effect of complexity on marine ecosystem models. Marine Ecology Progress Series 253, 1–16.

Fulton, E.A., Parslow, J.S., Smith, A.D.M., Johnson, C.R., 2004. Biogeochemical marine ecosystem models II: the effect of physiological detail on model performance. Ecological Modelling 173, 371–406.

Gentleman, W., Leising, A., Frost, B., Strom, S., Murray, J., 2003. Functional responses for zooplankton feeding on multiple resources: a review of assumptions and biological dynamics. Deep-Sea Research II 50, 2847–2875.

Gin, K.Y.H., Guo, J., Cheong, H.-F., 1998. A size-based ecosystem model for pelagic waters. Ecological Modelling 112, 53–72.

Goebel, N.L., Edwards, C.A., Zehr, J.P., Follows, M.J., 2010. An emergent community ecosystem model applied to the California Current System. Journal of Marine Systems 83, 221–241.

Hales, B., Moum, J.N., Covert, P., Perlin, A., 2005. Irreversible nitrate fluxes due to turbulent mixing in a coastal upwelling system. Journal of Geophysical Research 110, C10S11.

Hansen, B., Bjornsen, P.K., Hansen, P.J., 1994. The size ratio between planktonic predators and their prey. Limnology and Oceanography 39, 395–403.

Hansen, P.J., 1992. Prey size selection, feeding rates and growth dynamics of heterotrophic dinoflagellates with special emphasis on Gyrodinium spirale. Marine Biology 114, 327–334.

Hansen, P.J, Bjornsen, P.K., Hansen, B.W., 1997. Zooplankton grazing and growth: scaling within the 2–2000 μm body size range. Limnology and Oceanography 42, 697–704.

Hastings, A., Powell, T., 1991. Chaos in a three-species food chain. Ecology 72, 896–903.

Hawkins, E., Sutton, R., 2010. The potential to narrow uncertainty in projections of regional precipitation change. Climate Dynamics, http://www.springerlink.com/content/g3m4q2613571094j/.

Hickey, B.M., et al., 2010. River influences on shelf ecosystems: introduction and synthesis. Journal of Geophysical Research 115, (C00B17).

Huisman, J., Weissing, F.J., 1999. Biodiversity of plankton by species oscillations and chaos. Nature 402, 407–410.

Huisman, J., Weissing, F.J., 2001. Fundamental unpredictability in multispecies competition. The American Naturalist 157, 488–494.

Hutchinson, G.E., 1961. The paradox of the plankton. The American Naturalist 95, 137–145.

Irigoien, X., Huisman, J., Harris, R.P., 2004. Global biodiversity patterns of marine phytoplankton and zooplankton. Nature 429, 863–867.

Jacobson, D.M., 1999. A brief history of dinoflagellate feeding research. Journal of Eukaryotic Microbiology 46, 376–381.

Kondoh, M., 2003. Foraging adaptation and the relationship between food-web complexity and stability. Science 299, 1388–1391.

Litchman, E., Klausmeier, C.A., Yoshiyama, K., 2009. Contrasting size evolution in marine and freshwater diatoms. Proceedings of the National Academy of Sciences of the United States of America 106, 2665–2670.

Mariani, P., Visser, A.W., 2010. Optimization and emergence in marine ecosystem models. Progress in Oceanography 84, 89–92.

May, R., 1976. Simple mathematical models with very complicated dynamics. Nature 261, 459–467.

McCann, K., Hastings, A., Huxel, G.R., 1998. Weak interactions and the balance of nature. Nature 395, 794–798.

Moloney, C.L., Field, J.G., 1991. The size-based dynamics of plankton food webs. I. A simulation model of carbon and nitrogen flows. Journal of Plankton Research 13, 1003–1038.

Olson, M.B., Lessard, E.J., Cochlan, W.P., Trainer, V.L., 2008. Intrinsic growth and microzooplankton grazing on toxigenic Pseudo-nitzschia spp. diatoms from the coastal northeast Pacific. Limnology and Oceanography 53, 1352–1368.

Plattner, G.-K., Gruber, N., Frenzel, H., McWilliams, J.C., 2005. Decoupling marine export production from new production. Geophysical Research Letters 32 (L11612).

Post, D.M., Conners, M.E., Goldberg, D.S., 2000. Prey preference by a top predator and the stability of linked food chains. Ecology 81, 8–14.

Poulin, F.J., Franks, P.J.S., 2010. Size-structured planktonic ecosystems: constraints, controls and assembly instructions. Journal of Plankton Research 32, 1121–1130.

Schartau, M, Landry, M.R., Armstrong, R.A., 2010. Density estimation of plankton size spectra: a reanalysis of IronEx II data. Journal of Plankton Research 32, 1167–1184.

Sheldon, R.W., Prakash, A., Sutcliffe, W.H., 1972. The size distribution of particles in the ocean. Limnology and Oceanography 17, 327–340.

Sournia, A., Chrétiennot-Dinet, M.-J., Ricard, M., 1991. Marine phytoplankton: how many species in the world ocean? Journal of Plankton Research 13, 1093–1099.

Stock, C.A., Powell, T.M., Levin, S.A., 2008. Bottom-up and top-down forcing in a simple size-structured plankton dynamics model. Journal of Marine Systems 74, 134–152.

Stoecker, D., Guillard, R.R.L., Kavee, R.M., 1981. Selective predation by *Favella ehrenbergii* (Tintinnia) on and among dinoflagellates. Biological Bulletin 160, 136–145.

Tang, E.P.Y., 1995. The allometry of algal growth rates. Journal of Plankton Research 17, 1325–1335.

Tebaldi, C., Knutti, R., 2007. The use of the multi-model ensemble in probabilistic climate projection. Philosophical Transactions of the Royal Society A 365, 2053–2075.
Troost, T.A., Kooi, B.W., Dieckmann, U., 2008. Joint evolution of predator body size and prey-size preference. Evolutionary Ecology 22, 771–799.
Weitz, J.S., Levin, S.A., 2006. Size and scaling of predator–prey dynamics. Ecology Letters 9, 548–557.
Williams, R.J., 2008. Effects of network and dynamical model structure on species persistence in large model food webs. Theoretical Ecology 1, 141–151.
Zhou, M., Huntley, M.E., 1997. Population dynamics theory of plankton based on biomass spectra. Marine Ecology Progress Series 159, 61–73.